

Many-body shake-up in Auger neutralization of slow Ar⁺ ions at Al surfaces

A. Sindona,¹ R. A. Baragiola,² G. Falcone,¹ A. Oliva,¹ and P. Riccardi^{1,2,*}

¹*Dipartimento di Fisica, Università della Calabria and INFN, Gruppo Collegato di Cosenza, Via P. Bucci, Cubo 30C, 87036 Rende (CS), Italy*

²*Engineering Physics, University of Virginia, Thornton Hall, Charlottesville, Virginia 22901, USA*

(Received 2 July 2004; published 31 May 2005)

Electron emission by 130–430-eV Ar⁺ ion impact on polycrystalline Al surfaces is studied extending the theory of Auger neutralization to include the singular response of the metal conduction band to the sudden change of charge in the incoming hole state, following its neutralization. The effect is manifested in the high-energy tail of the electron energy distributions, where the theory accounts very well with experiments.

DOI: 10.1103/PhysRevA.71.052903

PACS number(s): 79.20.Rf, 34.50.Dy, 34.70.+e, 71.10.–w

I. INTRODUCTION

Neutralization of ions at the surface of a solid converts the potential energy carried by incoming projectiles into electron excitation and emission. Since the theoretical foundations laid by Hagstrum [1], potential electron emission (PEE) has been long discussed in terms of two-electron, Auger-type processes, such as Auger neutralization (AN) and resonant neutralization followed by interatomic Auger de-excitation (RN+AD) [1–4]. In AN, the electrostatic repulsion between two target electrons leads to one of the electrons tunneling to neutralize the incoming ion, and the other being excited. Recent studies have shown that the energy released by ion neutralization at metal targets can also produce collective excitations in the conduction band, such as surface plasmons, whose decay occurs predominantly by excitation of a single conduction electron (*plasmon-assisted neutralization* [5]). From this perspective, understanding how the potential energy of an incoming ion is transferred to the solid relates to important aspects of fundamental physics. Furthermore, slow ions neutralized outside the target provide a unique probe for electronic excitations confined just to the surface region, making the spectroscopy of emitted electrons one of the most surface sensitive tools to study solids.

In this paper, we reconsider the theory of AN for slow, singly charged, positive ions at metal targets and discuss another collective excitation, known as *Fermi edge singularity* [6]: the sudden change of charge of the projectile leads to a rearrangement of the ground state of conduction electrons on a long time scale; this final-state effect parallels the sudden creation of a core hole by absorption of a soft x-ray photon [6,7] and reflects in the broadening of the distributions of ejected electrons with kinetic energy E , for a given incident ion velocity.

We present measurements (Sec. II) and calculations (Secs. III and IV) showing that each distribution is broadened by the following components:

- (i) asymptotic behavior of the matrix elements of the Auger potential;
- (ii) initial-state lifetime;

- (iii) final-state lifetime;
- (iv) shift in atomic energy of the projectile near the surface;
- (v) shift of the Fermi surface in the reference frame of the projectile;
- (vi) electron-phonon interaction at room temperature;
- (vii) nonorthogonality between initial and final states due to the sudden switching of a localized potential in the neutralized ion.

Effects (i)–(vi) have already been recognized and extensively studied [1,7]; specifically, components (i) and (iii) produce a dominant Lorentzian broadening, yielding a common intersection point (i.e., a “*magic energy*”) for spectra acquired at different ion kinetic energies [2]. The Fermi edge singularity (vii) can be treated by the theory of Mahan, Nozieres, and De Dominicis (MND) [6] developed for x-ray studies [7].

We measured the kinetic energy distributions of electrons during the impact on Al surfaces of 130–430-eV Ar⁺ ions (Sec. II), whose neutralization is not mediated by plasmon excitation [5] and involves only the ground state of the projectiles. In fact, although far from the surface the energies of lowest excited states of Ar are nearly degenerate with the Fermi energy of Al, the interaction with the surface yields a positive shift of about 1.5 eV, making negligible the probability for RN+AD processes. We observed that inclusion of the Fermi edge singularity is needed to adequately reproduce the high-energy behavior of the spectra (Secs. III–V).

II. EXPERIMENTS

The experimental setup was described previously [5]: Ar⁺ ions were produced in an electron bombardment source operated at low electron energies (30 eV) to prevent significant contamination of the ion beam with doubly charged ions. The surface of the samples were normal to the axis of the spectrometer and at 12° with respect to the ion beam direction. The spectrometer was operated at a constant pass energy of 50 eV (and therefore an approximately constant transmission over the measured electron energy range) and with a resolution of 0.2 eV. The high-purity polycrystalline Al surfaces were sputter cleaned by 4-keV Ar⁺ ions at 12° glancing incidence.

The spectra were acquired with the sample biased at –2.5 V to separate the contribution of electrons emitted di-

*Electronic address: Riccardi@fis.unical.it

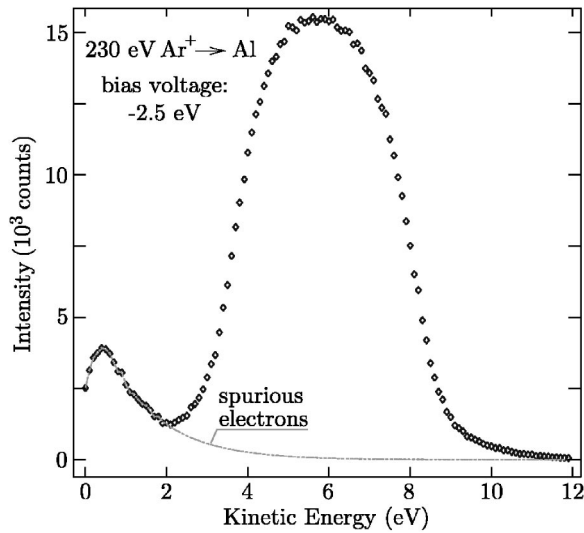


FIG. 1. Kinetic energy distribution of electrons ejected from Al by 230-eV Ar^+ ions, with the sample biased at -2.5 V.

rectly from the sample (and accordingly shifted to higher energies) from a spurious peak of low energy electrons, mainly arising from the grounded entrance grid of the analyzer, that tails exponentially and can be easily subtracted (Fig. 1). The adequacy of this procedure can be seen by comparison with the spectra acquired without the bias voltage (Fig. 2).

The *corrected* energy distributions of emitted electrons (Fig. 3), show the characteristic features of AN spectra [1–4]: constant areas, i.e., total electron emission yields, and a magic energy. At emission energies larger than the 5.3 eV magic value, each spectrum follows an exponential trend. This behavior cannot be ascribed to electrons ejected by kinetic energy transfer from the projectile, since previous measurements—of 1 keV Ar^+ impact on Al surfaces at varying incident angle [5]—have shown that their contribution

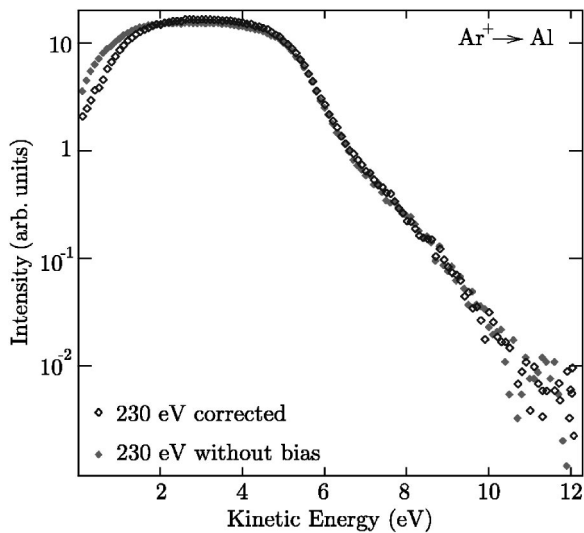


FIG. 2. Corrected distribution of Fig. 1, shifted backwards by the bias voltage, and spectrum acquired without the bias voltage. The spectra are normalized to the same height.

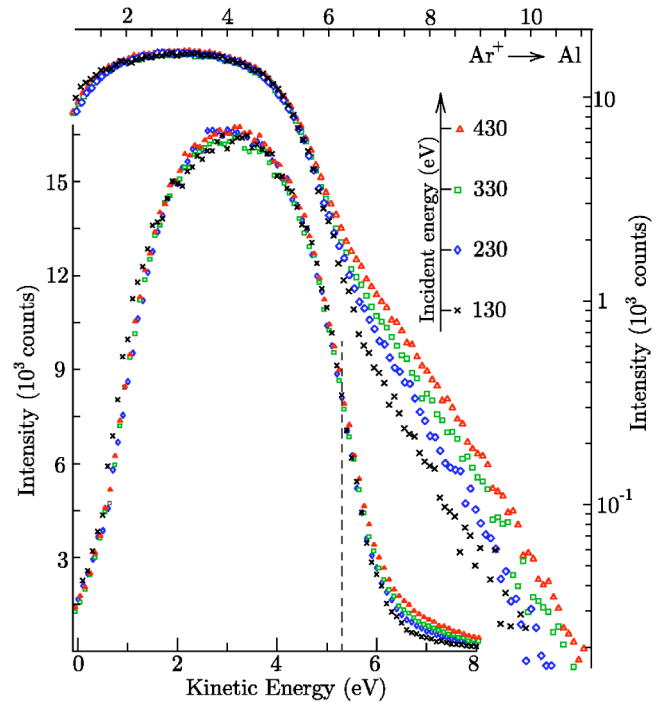


FIG. 3. (Color online) Kinetic energy distributions of electrons ejected from Al by 130–430-eV Ar^+ ions.

does not affect significantly the high-energy broadening of the electron spectra. Furthermore, the exponential tailing cannot be explained in terms of the mechanism (i)–(vi), suggesting presence of another broadening effect that will be explained in terms of the Fermi edge singularity (vii).

III. THEORY

We reexamine the basic interactions in a many electron system probed by the positively charged background of the atomic cores of the ion-metal structure and, unless stated otherwise, we use atomic units.

A. Hamiltonian

Let \mathbf{R} denote the position vector of the projectile in a reference frame at the surface of the metal. Each electron at position \mathbf{r} interacts independently with the external potential,

$$v_E(\mathbf{r}, \mathbf{R}) = v_S(z) + v_A(\mathbf{r} - \mathbf{R}) + \Delta v_A(\mathbf{r}, \mathbf{R}), \quad (3.1)$$

where $v_S(z)$ is the surface barrier of the metal band [8], $v_A(\mathbf{r} - \mathbf{R})$ the effective central field of the impinging ion [9], and $\Delta v_A(\mathbf{r}, \mathbf{R})$ the change of the surface potential induced by the positive ion charge [10,11]. Thus the single-particle part of the Hamiltonian writes $h_E(\mathbf{r}, \mathbf{R}) = -\nabla^2/2 + v_E(\mathbf{r}, \mathbf{R})$ and the electrostatic repulsion between two electrons, at positions \mathbf{r} and \mathbf{r}' , respectively, is described by a central potential of the form $v_{SC}(|\mathbf{r} - \mathbf{r}'|)$ that takes into account the screening of other electrons in the medium.

In this spinless approach, the total Hamiltonian is written in second quantization as

$$\begin{aligned}\mathcal{H}(\mathbf{R}) &= \int d^3r \Psi^\dagger(\mathbf{r}, \mathbf{R}) h_E(\mathbf{r}, \mathbf{R}) \Psi(\mathbf{r}, \mathbf{R}) \\ &= \frac{1}{2} \int d^3r \int d^3r' \Psi^\dagger(\mathbf{r}, \mathbf{R}) \Psi^\dagger(\mathbf{r}', \mathbf{R}) \\ &\quad \times v_{\text{SC}}(|\mathbf{r} - \mathbf{r}'|) \Psi(\mathbf{r}', \mathbf{R}) \Psi(\mathbf{r}, \mathbf{R}).\end{aligned}\quad (3.2)$$

Here $\Psi(\mathbf{r}, \mathbf{R})$, the electron field operator in real space, can be expanded over the truncated orthonormal set $\{|\mathbf{r}|k\rangle\}$ of the metal Hamiltonian $h_M(z) = -\nabla^2/2 + v_S(z)$, with spectrum $\{\varepsilon_k\}$, and the eigenfunction $\langle \mathbf{r}|a_0(\mathbf{R})\rangle = \langle \mathbf{r} - \mathbf{R}|a_0\rangle$ of the atomic Hamiltonian $h_A(\mathbf{r} - \mathbf{R}) = -\nabla^2/2 + v_A(\mathbf{r} - \mathbf{R})$, with eigenenergy ε_a^∞ . $h_M(z)$ characterizes the conduction band, of Fermi energy ε_F —wave vector k_F —and width ξ , including the continuous spectrum above the vacuum level and below ~ 10 eV, while $h_A(\mathbf{r} - \mathbf{R})$ corresponds to the single atomic level active for neutralization.

Atomic and metal states are *orthonormalized* as the ion approaches the vicinity of the surface [3] by introducing the wave function $\langle \mathbf{r}|a(\mathbf{R})\rangle = \langle \mathbf{r}|a_0(\mathbf{R})\rangle - \sum_k \langle \mathbf{r}|k\rangle \langle k|a_0(\mathbf{R})\rangle$ such that

$$\Psi(\mathbf{r}, \mathbf{R}) = \sum_k \langle \mathbf{r}|k\rangle c_k + \langle \mathbf{r}|a(\mathbf{R})\rangle c_a(\mathbf{R}) \quad (3.3)$$

and annihilations operators $\{c_k\} \cup \{c_a(\mathbf{R})\}$ satisfy the ordinary algebraic rules of fermion operators.

Substituting the expansion (3.3) into (3.2) yields

$$\mathcal{H}(\mathbf{R}) = \mathcal{H}_0(\mathbf{R}) + \mathcal{V}_H(\mathbf{R}) + \mathcal{V}_{\text{AU}}(\mathbf{R}) + \mathcal{V}_{\text{FE}}(\mathbf{R}) \quad (3.4)$$

in which

$$\mathcal{H}_0(\mathbf{R}) = \varepsilon_a(\mathbf{R}) c_a^\dagger(\mathbf{R}) c_a(\mathbf{R}) + \sum_k \varepsilon_k c_k^\dagger c_k \quad (3.5)$$

refers to the unperturbed electron gas in the truncated orthonormal set $\{|\mathbf{r}|k\rangle\} \cup \{|\mathbf{r}|a(\mathbf{R})\}$ with spectrum $\{\varepsilon_k\} \cup \{\varepsilon_a(\mathbf{R})\} = \langle a(\mathbf{R})|h_E(\mathbf{r}, \mathbf{R})|a(\mathbf{R})\rangle$;

$$\mathcal{V}_H(\mathbf{R}) = \sum_k \{V_{ak}(\mathbf{R}) c_a^\dagger(\mathbf{R}) c_k + \text{H.c.}\}, \quad (3.6)$$

is the one-body hopping potential of for resonant charge transfer [12], of matrix elements $V_{ak}(\mathbf{R}) = \langle a(\mathbf{R})|h_E(\mathbf{r}, \mathbf{R})|k\rangle$;

$$\mathcal{V}_{\text{AU}}(\mathbf{R}) = \sum_{k, k', k''} \{V_{kk'}^{ak''}(\mathbf{R}) c_a^\dagger(\mathbf{R}) c_k^\dagger c_{k'} c_{k''} + \text{H.c.}\} \quad (3.7)$$

denotes the usual Auger potential [1–4] of matrix elements $V_{kk'}^{ak''}(\mathbf{R}) = \langle k|\langle a(\mathbf{R})|v_{\text{SC}}(|\mathbf{r} - \mathbf{r}'|)|k''\rangle|k'\rangle$; and

$$\mathcal{V}_{\text{FE}}(\mathbf{R}) = \sum_{k, k'} V_{kk'}^a(\mathbf{R}) c_k^\dagger c_{k'} c_a^\dagger(\mathbf{R}) c_a(\mathbf{R}) \quad (3.8)$$

is a new interaction, of matrix elements $V_{kk'}^a(\mathbf{R}) = \langle k|\langle a(\mathbf{R})|v_{\text{SC}}(|\mathbf{r} - \mathbf{r}'|)|a(\mathbf{R})\rangle|k'\rangle$, that describes the sudden change of charge due to neutralization of the incident ion and injection of a band hole. It has the same structure of the MND potential, where $c_a^\dagger c_a$ is the number operator of the core hole [6].

Other interactions such as the one-body intraband scattering potential of metal electrons, of matrix elements $V_{kk'} = \langle k|v_E(\mathbf{r}, \mathbf{R})|k'\rangle$, and the two-body electron-electron potential between the band states, of matrix elements $V_{kk''}^{k'k''} = \langle k|\langle k'|v_{\text{SC}}(|\mathbf{r} - \mathbf{r}'|)|k''\rangle|k'''\rangle$, are neglected. The latter needs to be considered when the plasmon-assisted neutralization channel—arising from the dynamic screening by the metal electrons [4]—is active, which is not the case of Ar^+/Al where the energy released by neutralization is insufficient to excite even a $q=0$ surface plasmon [5].

The exactly solvable part of the reference Hamiltonian (3.2) is $\mathcal{H}'_0(\mathbf{R}) = \mathcal{H}_0(\mathbf{R}) + \mathcal{V}_{\text{FE}}(\mathbf{R})$ that introduces a partition of the Fock space into two subspaces: on the one hand, many electron states with the ion state empty are still constructed by antisymmetrizing the unperturbed set $\{|\mathbf{r}|k\rangle\}$; on the other hand, many electron states with the ion state occupied need to be calculated from the eigenfunctions $\{|\mathbf{r}|k_a(\mathbf{R})\}$ of the final-state Hamiltonian $h'_M(z) = h_M(z) + v_{\text{FE}}(\mathbf{r}, \mathbf{R})$, with the same spectrum of the unperturbed operator $h_M(z)$. The one-electron potential activated by neutralization reads

$$v_{\text{FE}}(\mathbf{r}, \mathbf{R}) = \int d^3r' v_{\text{SC}}(\mathbf{r} - \mathbf{r}') |\langle \mathbf{r}'|a(\mathbf{R})\rangle|^2, \quad (3.9)$$

and the final states of AN are nonorthogonal to the initial state.

B. Fermi's golden rule formulation

The trajectory followed by the projectile is handled classically, thus the dynamic of the system is parametrically time dependent. In the simplest case, the ion can be assumed to reflect elastically from a plane at distance Z_0 from surface of the target, moving along a straight line $\mathbf{R} = \mathbf{R}(t)$ of incident velocity $\mathbf{v} = (v_{\parallel}, v_{\perp})$, parallel component $\mathbf{R}_{\parallel}(t) = \mathbf{v}_{\parallel} t$ and perpendicular component $Z(t) = v_{\perp} |t| + Z_0$. Since complete knowledge of the eigenfunctions of both $h_M(z)$ and $h'_M(z)$ is available, we work in the interaction picture spanned by $\mathcal{H}'_0[\mathbf{R}(t)]$ and treat the Auger potential $\mathcal{V}_{\text{AU}}[\mathbf{R}(t)]$ of Eq. (3.7) as a small perturbation [14].

The key quantity in our study is the transition rate, $1/\tau_a(\varepsilon_k, \mathbf{v})$, from the unperturbed ground state of the conduction band $|0\rangle_N$, composed of N band electrons with the ion state empty, to all possible excited states $|f_a[\varepsilon_k, \mathbf{R}(t)]\rangle_N$, with $N-2$ electrons below the Fermi energy, the ion state occupied, and an excited electron with energy $\varepsilon_k > \varepsilon_F$. The initial state is the ground state of $\mathcal{H}_0[\mathbf{R}(t)]$ —with eigenenergy E_0 —and each final state diagonalizes $\mathcal{H}'_0[\mathbf{R}(t)]$ —with eigenenergy $E_f^a[\mathbf{R}(t)]$. By Fermi's golden rule,

$$\begin{aligned}\frac{1}{\tau_a}(\varepsilon_k, \mathbf{v}) &= 2\pi \int_{-\infty}^{\infty} dt \sum_f e^{i\int_0^t dt' \{E_f^a[\mathbf{R}(t')] - E_0\}} \\ &\quad \times |\langle f_a[\varepsilon_k, \mathbf{R}(t)]|\mathcal{V}_{\text{AU}}[\mathbf{R}(t)]|0\rangle_N|^2.\end{aligned}\quad (3.10)$$

The MND potential (3.8) modifies significantly the many electron states of the metal, when the atomic level is occupied, while it acts as a weak perturbation on single-particle states. Figure 3 shows that a new broadening mechanism is

needed to explain the behavior of the energy tails of experimental electron energy distributions, above the magic energy. Thus we intend to evaluate the effect of the Fermi edge singularity at the edge of AN, i.e., when the electrons of the initial state, that participate to the process, lie close to the Fermi energy. In this case, both the atomic and the excited electron, in the final state, are negligibly perturbed by the one electron potential (3.9), since their energies, relative to the Fermi energy, are large on the eV scale. For these reasons, we can approximate

$$|f_a[\varepsilon_k, \mathbf{R}(t)]\rangle_N \approx c_k^\dagger c_a^\dagger[\mathbf{R}(t)]|f[\mathbf{R}(t)]\rangle_{N-2}, \quad (3.11)$$

in which $|f[\mathbf{R}(t)]\rangle_{N-2}$ is an excited state of the metal, with time-independent eigenenergy E_f , that involves the $N-2$ band electron that do not participate to AN.

Using Eq. (3.11) into Eq. (3.10), and approximating the energy of the band holes created by AN to ε_F , we obtain (see the Appendix)

$$\begin{aligned} \frac{1}{\tau_a}(\varepsilon_k, \mathbf{v}) &= 2\pi\rho(\varepsilon_k) \int d^2\Omega_k \sum_{k', k''} \int_{-\infty}^{\infty} dt |V_{kk'}^{ak''}[\mathbf{R}(t)]|^2 \\ &\times F_a(\mathbf{v}, t) e^{i\int_0^t dt' \{\varepsilon_k + \varepsilon_a[\mathbf{R}(t')] - \varepsilon_{k'} - \varepsilon_{k''}\}}, \end{aligned} \quad (3.12)$$

where $\rho(\varepsilon_k)$ is the density of final states available to excited electrons,

$$F_a(\mathbf{v}, t) = {}_{N-2}\langle 0 | c_a[\mathbf{R}(0)] \mathcal{U}(\mathbf{v}; 0, t) c_a^\dagger[\mathbf{R}(t)] | 0 \rangle_{N-2} \quad (3.13)$$

is the propagator for the atomic electron, in the ground state of the $N-2$ band electrons that do not participate to AN, and $\mathcal{U}(\mathbf{v}; 0, t)$ is the time-development operator for the singular potential (3.8), in the interaction picture spanned by the free-electron-gas Hamiltonian (3.5).

The next step is the determination of $N_1(\varepsilon_k, \mathbf{v})$, the distribution of electrons excited above the Fermi level by the incident ion, being proportional to Eq. (3.12) that we reexpress in the reference frame moving with the constant parallel velocity of the projectile,

$$\begin{aligned} \frac{1}{\tau_a}(\varepsilon_k, \mathbf{v}) &= 2\pi\rho(\varepsilon_k) \int d^2\Omega_k \sum_{k', k''} \int_{-\infty}^{\infty} dt |V_{kk'}^{ak''}[Z(t)]|^2 \\ &\times e^{i\int_0^t dt' \{\varepsilon_k + \varepsilon_a[Z(t')] - \varepsilon_{k'} - \varepsilon_{k''} - \mathbf{q} \cdot \mathbf{v}_{\parallel}\}} F_a(v_{\perp}, t). \end{aligned} \quad (3.14)$$

In this relationship, $\mathbf{q} = \mathbf{k} - \mathbf{k}' - \mathbf{k}''$ labels the momentum exchanged in a single excitation process and the factor $e^{-i\mathbf{q} \cdot \mathbf{v}_{\parallel}}$ accounts for the shift of the Fermi surface in the moving frame (\mathbf{v}).

Then, we need to consider effects that are outside Fermi golden's rule formulation, i.e., the lifetime of initial (ii) and final (iii) states and the effect of the electron-phonon interaction at room temperature (vi). We introduce the probability that the ion ground state survives neutralization, due to both Auger and resonant transitions

$$P_a(v_{\perp}, t) = e^{-\int_{-\infty}^t dt' \{(1/\tau_a') [Z(t')] + 2\Delta_a[Z(t')]\}}, \quad (3.15)$$

which includes the total AN transition rate [1,2]

$$\frac{1}{\tau_a'}(Z) = 2\pi \sum_{k, k', k''} \int_{-\infty}^{\infty} dt |V_{kk'}^{ak''}(Z)|^2 \delta[\varepsilon_a(Z) + \varepsilon_k - \varepsilon_{k'} - \varepsilon_{k''}] \quad (3.16)$$

and the virtual width of the atomic state [11,12] via hopping processes

$$\Delta_a(Z) = \sum_k |V_{ak}(Z)|^2 \delta[\varepsilon_a(Z) - \varepsilon_k]. \quad (3.17)$$

Finally, we take a simple exponential law, with average lifetime Γ_0 , for the probability that the band holes created by AN survive recombination [1] and we model the electron-phonon interaction by a Gaussian function of width σ_{PH} [7].

With these prescriptions, we can write

$$\begin{aligned} N_1(\varepsilon_k, \mathbf{v}) &= N_0 \rho(\varepsilon_k) \int d^2\Omega_k \sum_{k', k''} \int_{-\infty}^{\infty} dt |V_{kk'}^{ak''}[Z(t)]|^2 \\ &\times F_a(v_{\perp}, t) P_a(v_{\perp}, t) e^{-\Gamma_0 t - \sigma_{\text{PH}}^2 t^2 / 2} \\ &\times e^{i\int_0^t dt' \{\varepsilon_k + \varepsilon_a[Z(t')] - \varepsilon_{k'} - \varepsilon_{k''} - \mathbf{q} \cdot \mathbf{v}_{\parallel}\}}, \end{aligned} \quad (3.18)$$

where the new effect, i.e., the Fermi edge singularity (vii), is contained in the propagator (3.13).

By Eq. (3.18), $N_1(\varepsilon_k, \mathbf{v})$ can be expressed as the convolution product

$$N_1(\varepsilon_k, \mathbf{v}) = \int_{-\infty}^{\infty} dx N_1^0(\varepsilon_k, \varepsilon_k - x, \mathbf{v}) B(x, v_{\perp}), \quad (3.19)$$

in which

$$\begin{aligned} N_1^0(\varepsilon_k, \varepsilon, \mathbf{v}) &= N_0 \int d^2\Omega_k \sum_{k', k''} u_{kk'}^{ak''} [\varepsilon + \varepsilon_a(Z_0) - \varepsilon_k \\ &- \varepsilon_{k''} - \mathbf{q} \cdot \mathbf{v}_{\parallel}] \end{aligned} \quad (3.20)$$

is the spectrum of excited electrons broadened by the Auger potential (i), via the *internal functions*

$$u_{kk'}^{ak''}(\varepsilon) = \rho(\varepsilon_k) \int_{-\infty}^{\infty} \frac{dt}{2\pi} e^{i\varepsilon t} |V_{kk'}^{ak''}[Z(t)]|^2, \quad (3.21)$$

and

$$\begin{aligned} B(\varepsilon, v_{\perp}) &= \int_{-\infty}^{\infty} dt e^{i(\varepsilon - \Gamma_0)t - \sigma_{\text{PH}}^2 t^2 / 2} F_a(v_{\perp}, t) \\ &\times P_a(v_{\perp}, t) e^{i\int_0^t dt' \{\varepsilon_a[Z(t')] - \varepsilon_a(Z_0)\}} \end{aligned} \quad (3.22)$$

denotes the broadening function for mechanisms (ii)–(vii).

For normal emission, the distribution of electrons ejected from the metal writes

$$N(E, \mathbf{v}) = T(E) N_1(E, \mathbf{v}). \quad (3.23)$$

It depends on the electron kinetic energy outside the solid $E = \varepsilon_k - \xi$ and is related to the distribution of excited electrons via the escape probability or surface transmission function [13],

$$T(E) = \Theta(E) \frac{E}{E + \xi}. \quad (3.24)$$

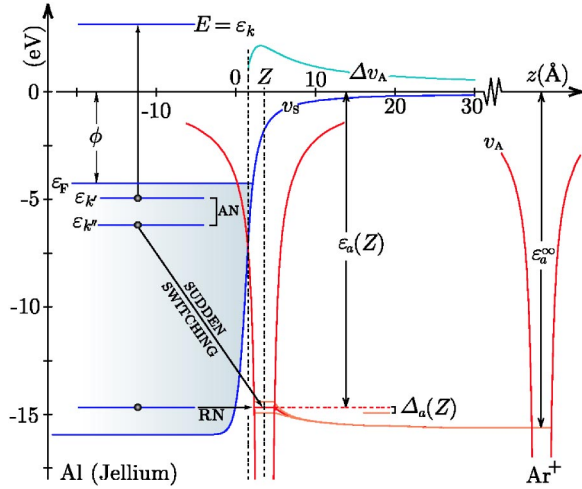


FIG. 4. (Color online) Schematics of AN from the Ar^+/Al system.

IV. APPLICATION

We apply Eqs. (3.20) and (3.22) to Ar^+/Al , using $\varepsilon_F = -\phi = -4.25$ eV, $k_F = 0.93$ au, $\xi = 15.95$ eV, and $\varepsilon_a^\infty = -15.76$ eV, where energies are measured relative to the vacuum level and therefore $E = \varepsilon_k$ (Fig. 4). We approximate the electron-electron potential to the Yukawa form,

$$v_{\text{SC}}(|\mathbf{r} - \mathbf{r}'|) = \frac{e^{-\mu|\mathbf{r} - \mathbf{r}'|}}{|\mathbf{r} - \mathbf{r}'|}, \quad (4.1)$$

in which μ is the inverse screening length of the electron gas. Thus the matrix elements $V_{kk'}^{ak''}$ and $V_{kk'}^a$ can be worked out by Fourier transforming in the coordinates parallel to the surface [2] and numerically integrating over the coordinates perpendicular to the surface. $N_1^0(E, \mathbf{v})$ can be obtained using Monte Carlo techniques for multiple wave-vector integrals over Ω_k , k' and k'' in Eq. (3.20), where the internal functions $u_{kk'}^{ak''}(\varepsilon)$ are calculated from the numerical Fourier transform of $|V_{kk'}^{ak''}[Z(t)]|^2$.

The basic theory of AN corresponds to the replacement $F_a(v_\perp, t) \rightarrow 1$ in Eqs. (3.18) and (3.22), which leads the external distributions $N(E, \mathbf{v})$ to depend on four parameters: Z_0 , σ_{PH} , μ , and Γ_0 . Z_0 is determined by the constraint that the external distributions coincide at the experimental magic energy, yielding $Z_0 = 4$ Å, and for σ_{PH} we use the same value of x-ray studies on Al at room temperature, i.e., $\sigma_{\text{PH}} \sim 0.1$ eV [7]. Indeed, adjustment with the experiments of all the four parameters confirmed the estimates for Z_0 and σ_{PH} , and yielded $\mu = 0.1 k_F$ and $\Gamma_0 = 0.05$ eV. Variation of μ has a strong influence on the position of the peak of $N_1(\varepsilon_k, \mathbf{v})$, that for $\mu \leq 1.00 k_F$ lies at $\varepsilon_k \leq -2$ eV, below the vacuum level. However, it has a weaker influence on the high-energy tail of the internal distributions, at $\varepsilon_k \geq 1$ eV above the vacuum level, so that the external distribution $N(E, \mathbf{v})$ is not significantly affected at $E \geq 1$ eV. We verified by calculations that this is the case for any choice of μ in the range $0.05 k_F \leq \mu \leq 1.00 k_F$. Therefore Γ_0 is the only parameter that needs to be fitted. The value reported above lies in the range 0.01–0.1

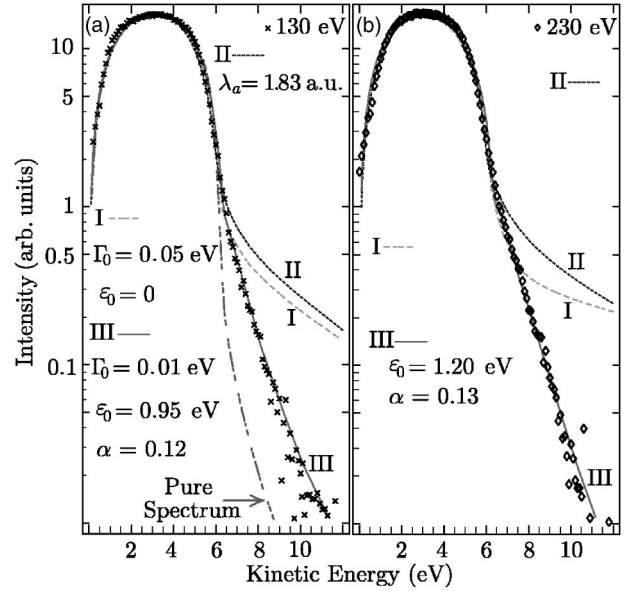


FIG. 5. Electron spectra of Fig. 3, for the ion incident energies 130–230 eV, are compared with theoretical distributions calculated from (I) the basic theory of AN; (II) Hagstrum's model, and (III) Eqs. (3.20) and (3.22).

eV, estimated by the theory of mean free paths of hot holes in solids [1].

This choice of the four parameters corresponds to the distributions of Figs. 5 and 6, broadened by the experimental energy resolution and labeled I. In the same figures are shown the experimental spectra and the distributions II obtained from Hagstrum's convolution model [1] that we derived in our formulation by neglecting the effect of \mathbf{v}_\parallel and using the approximated factorization

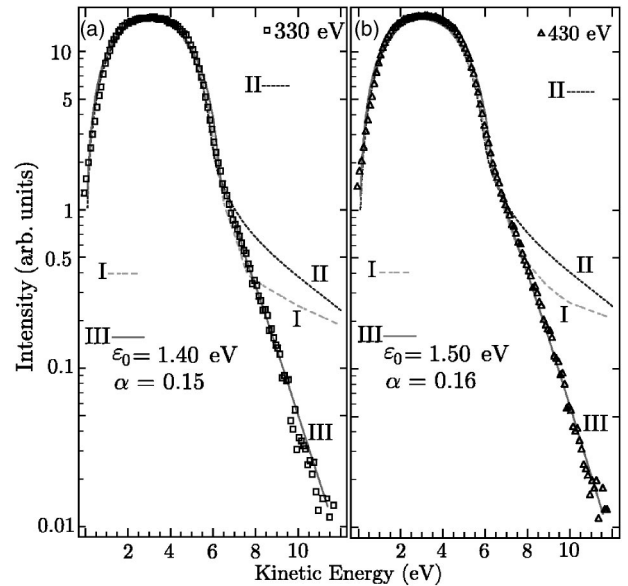


FIG. 6. Electron spectra of Fig. 3, for the ion incident energies 330–430 eV, are compared with theoretical distributions calculated from (I) the basic theory of AN, (II) Hagstrum's model, and (III) Eqs. (3.20) and (3.22).

$$V_{kk'}^{ak''}[Z(t)] \approx V_{kk'}^{ak''}(Z_0)e^{-\lambda_a v_\perp |t|/2}. \quad (4.2)$$

λ_a is determined from the average asymptotic slope of $\ln|V_{kk'}^{ak''}(Z)|^2$ over occupied band states, yielding $\lambda_a = 1.83$ a.u., which introduces a *universal* broadening function of the ion perpendicular velocity and the atomic level convolution of $B(\varepsilon_k, v_\perp)$ with a Lorentzian of constant width $\lambda_a v_\perp$. The approximated results II, for the same choice of Z_0 , μ , σ_{PH} , and Γ_0 , do not differ significantly from the numerical curves I. In fact, the ion velocity is always less than ~ 0.02 a.u., while the target Fermi velocity is 0.93 a.u. Consequently, the effective occupation of the target states in the rest frame at velocity \mathbf{v}_\parallel is very well described by the Fermi-Dirac distribution and shifted Fermi surface effects are small. Furthermore, each $|V_{kk'}^{ak''}(Z)|^2$ follows a strict exponential law at ion-surface distances typically larger than ~ 15 Å.

In either case, theoretical calculations (I, II) are in excellent agreement with the main part of experimental distributions of Fig. 3 for electron kinetic energies less than ~ 6 eV. However, the logarithmic scale evidences that the high-energy exponential behavior of spectra cannot be reproduced with the known broadening mechanisms.

The MND theory [6,7] predicts an asymmetric line shape of the form

$$F_{\text{MND}}(E') = \Theta(E') \frac{e^{-E'/\varepsilon_0}}{\Gamma(\alpha) \varepsilon_0^\alpha E'^{\alpha-1}}, \quad (4.3)$$

for photoemitted electrons with energy E' , relative to the core-hole energy, where ε_0 is a cutoff parameter of the order of the conduction band width and α a singularity index. $F_{\text{MND}}(E')$ results from the Fourier transform of Eq. (3.13) for a contact core-hole potential perturbing band electrons in a range of width ε_0 from the Fermi energy [6,14]. In the present context, we considered a contact potential of the form (3.8) with the matrix elements

$$V_{kk'}^a(Z) = \begin{cases} V_{k_{\text{F}}k_{\text{F}}}^a(Z), & \text{if } |\varepsilon_k - \varepsilon_{k'}| \leq \varepsilon_0 \\ 0, & \text{otherwise} \end{cases}, \quad (4.4)$$

obtaining for the correlation function F_a the same structure of the Fourier transform of F_{MND} , i.e.,

$$F_a(v_\perp, t) \approx \left(\frac{1}{1 + i\varepsilon_0(v_\perp)t} \right)^{\alpha(v_\perp)}. \quad (4.5)$$

Such a function seems to be the right candidate to cope with the high-energy discrepancies of the Lorentzian broadening model. The singularity index depends on the Fourier transform $\phi_l(v_\perp, \varepsilon)$ of the instantaneous phase shifts [15] of the potential (3.9) at $\varepsilon = \varepsilon_{\text{F}}$,

$$\alpha(v_\perp) = \sum_l \frac{(2l+1)}{\pi^2} |\Phi_l(v_\perp, \varepsilon_{\text{F}})|^2. \quad (4.6)$$

Calculation of α , in the *S*-wave approximation, and adjustment ε_0 show that both parameters increase with increasing v_\perp . α ranges from 0.12 to 0.16, the same order of the estimated value for the singularity indices of the measured 2s and 2p core lines of Al [7], and $0.9 \leq \varepsilon_0 \leq 1.5$ eV.

The modified electron distributions III, determined with the numerical internal functions $u_{kk'}^{ak''}$ and reported in Figs. 5 and 6, offer the correct exponential trend at higher energies. We find that Γ_0 is now reduced to 0.01 eV, being consistent with the range of values reported in literature [1]. In Fig. 5(a), we also show the *true unbroadened spectrum* of the ion-metal system [1], i.e., the static response of the target to a projectile at a fixed distance Z_0 from the surface. The latter, defined by

$$N_0(E) = T(E)N_1^0(E, \mathbf{v} \rightarrow \mathbf{0}), \quad (4.7)$$

crosses other theoretical distributions at the magic energy, as predicted by Monreal and Apell [2].

V. CONCLUSIONS

In summary, we extended the theory of AN to include the effect of many-body shake-up of metal electrons due to the abrupt change of the surface potential caused by electron capture by the incident ion outside the surface. The effect is manifested in the high-energy tail of the electron energy distributions, where the theory accounts very well with measurements reported in this work and elsewhere [5]. As a corollary, we expect the effect to be absent in materials with a band gap. In such cases, although some form of shake-up will still occur, the effect on the electron energy distributions will be markedly different because of the absence of a Fermi-edge singularity.

APPENDIX: APPROXIMATIONS INVOLVED IN THE EVALUATION OF THE AN TRANSITION RATE

The approximation (3.11) is reasonable when the energies of both the excited and the atomic electrons in an Auger transition are such that

$$|\varepsilon_k - \varepsilon_{\text{F}}| \gg \varepsilon_0(v_\perp), \quad |\varepsilon_a(Z) - \varepsilon_{\text{F}}| \gg \varepsilon_0(v_\perp), \quad (A1)$$

where $\varepsilon_0(v_\perp)$ is the width of the broadening function (4.3), responsible for the effect (vii). In relation with the Ar^+/Al system, we have shown that the experimental distributions electrons, in Figs. 3, 5, and 6, are reproduced with $\varepsilon_0(v_\perp) \lesssim 1.5$ eV. In addition, the maximum shift to the binding energy of the ion level is about ~ 1.5 eV, corresponding to the turning distance $Z_0 \sim 4$ Å (Fig. 4). Thus $|\varepsilon_a(Z) - \varepsilon_{\text{F}}|$ is generally larger than 10 eV. As for the energy of the excited electron, Eq. (A1) is satisfied for $\varepsilon_k \gtrsim 5$ eV. This means that shake-up electrons participating to AN, in the initial state, have energies close to ε_{F} . Therefore we can limit our estimation to their effect on the energy distributions above ~ 5 eV, where the basic theory of AN is unable to reproduce the studied experiments.

Substituting Eqs. (3.7) and (3.11) in Eq. (3.10), we obtain

$$\begin{aligned} & N_{-2} \langle f(\mathbf{R}) | c_a(\mathbf{R}) c_k \mathcal{V}_{\text{AU}}(\mathbf{R}) | 0 \rangle_{\text{N}} \\ &= \sum_{k', k''} V_{kk'}^{ak''}(\mathbf{R}) N_{-2} \langle f(\mathbf{R}) | c_{k'} c_{k''} | 0 \rangle_{\text{N}} \end{aligned} \quad (A2)$$

since $\varepsilon_k > \varepsilon_{\text{F}}$. Then,

$$\begin{aligned} \frac{1}{\tau_a}(\varepsilon_k, \mathbf{v}) &= 2\pi\rho(\varepsilon_k) \int d^2\Omega_k \int_{-\infty}^{\infty} dt \sum_f e^{i(E_f - E_0)t} \\ &\times e^{i\int_0^t dt' \{\varepsilon_a[\mathbf{R}(t')] + \varepsilon_k\}} \left| \sum_{k', k''} V_{kk'}^{ak''}[\mathbf{R}(t)] \right. \\ &\times \left. \langle \mathcal{N}_{-2} \langle f[\mathbf{R}(t)] | c_{k'} c_{k''} | 0 \rangle_{\mathcal{N}} \right|^2. \end{aligned} \quad (\text{A3})$$

By the completeness relation over the final states $\{|f[\mathbf{R}(t)]\rangle\}$, we can write

$$\sum_f |f[\mathbf{R}(t)]\rangle_{\mathcal{N}_{-2}} e^{iE_f t} \langle f[\mathbf{R}(t)]| = [\tilde{\mathcal{U}}_S(\mathbf{v}; 0, t)]_{\mathcal{N}_{-2}}, \quad (\text{A4})$$

where

$$\tilde{\mathcal{U}}_S(\mathbf{v}; t, 0) = \mathcal{T} e^{-i\int_0^t dt' \mathcal{K}'_0[\mathbf{R}(t')]} \quad (\text{A5})$$

is the time-development operator—in the Schrödinger representation—for the one-body Hamiltonian

$$\mathcal{K}'_0[\mathbf{R}(t)] = \sum_k \varepsilon_k c_k^\dagger c_k + \sum_{k, k'} V_{kk'}^a[\mathbf{R}(t)] c_k^\dagger c_{k'}, \quad (\text{A6})$$

and \mathcal{T} is the time ordering operator [16]. $[\tilde{\mathcal{U}}_S(\mathbf{v}; 0, t)]_{\mathcal{N}_{-2}}$ operates on the subspace of the $N-2$ metal electrons that do not participate to AN and \mathcal{K}_0 , the diagonal part of $\mathcal{K}'_0[\mathbf{R}(t)]$, is such that

$$e^{-iE_0 t} |0\rangle_{\mathcal{N}} = e^{-i\mathcal{K}_0 t} |0\rangle_{\mathcal{N}}. \quad (\text{A7})$$

Thus Eq. (A3) can be rewritten in the form

$$\begin{aligned} \frac{1}{\tau}(\varepsilon_k) &= 2\pi\rho(\varepsilon_k) \int d^2\Omega_k \int_{-\infty}^{\infty} dt e^{i\int_0^t dt' \{\varepsilon_k + \varepsilon_a[\mathbf{R}(t')\}} \\ &\times \sum_{k', k''} e^{-i(\varepsilon_{k'} + \varepsilon_{k''})t'} V_{kk'}^{ak''}[\mathbf{R}(t)] \\ &\times \sum_{\bar{k}', \bar{k}''} {}_a F_{\bar{k}'\bar{k}''}^{k'k''}(\mathbf{v}, t) V_{\bar{k}'\bar{k}''}^{\bar{k}'\bar{k}''}[\mathbf{R}(t)]. \end{aligned} \quad (\text{A8})$$

Here,

$${}_a F_{\bar{k}'\bar{k}''}^{k'k''}(\mathbf{v}, t) = {}_{\mathcal{N}} \langle 0 | c_{\bar{k}''}^\dagger c_{\bar{k}'}^\dagger \tilde{\mathcal{U}}(\mathbf{v}; 0, t) c_{\bar{k}'}(t) c_{\bar{k}''}(t) | 0 \rangle_{\mathcal{N}} \quad (\text{A9})$$

is the propagator for the core holes created by AN,

$$\tilde{\mathcal{U}}(\mathbf{v}; t, 0) = \mathcal{T} e^{i\mathcal{K}_0 t} \tilde{\mathcal{U}}_S(\mathbf{v}; t, 0) \quad (\text{A10})$$

the time-development operator (A5) in the interaction picture spanned by \mathcal{K}_0 , and $c_k(t) = e^{-i\varepsilon_k t} c_k$. By the linked cluster theorem [6,16], the many-body diagram (A9) can be written as

$${}_a F_{\bar{k}'\bar{k}''}^{k'k''}(\mathbf{v}, t) = L_{\bar{k}'\bar{k}''}^{k'k''}(\mathbf{v}, t) F_a(\mathbf{v}, t), \quad (\text{A11})$$

where

$$F_a(\mathbf{v}, t) = {}_{\mathcal{N}_{-2}} \langle 0 | \tilde{\mathcal{U}}(\mathbf{v}; 0, t) | 0 \rangle_{\mathcal{N}_{-2}} \quad (\text{A12})$$

can be interpreted as atomic electron propagator in the ground state of a metal band with $N-2$ electrons. In fact, it can be put in the form

$$F_a(\mathbf{v}, t) = {}_{\mathcal{N}_{-2}} \langle 0 | c_a[\mathbf{R}(0)] \mathcal{U}(\mathbf{v}; 0, t) c_a^\dagger[\mathbf{R}(t)] | 0 \rangle_{\mathcal{N}_{-2}}, \quad (\text{A13})$$

with $\mathcal{U}(\mathbf{v}; t, 0)$ the time development operator for $\mathcal{H}'_0[\mathbf{R}(t)]$, in the interaction picture spanned by $\mathcal{H}_0[\mathbf{R}(t)]$. Equation (A12) converges to Eq. (4.5) for the contact potential (4.4).

In the same approximation, $L_{\bar{k}'\bar{k}''}^{k'k''}(\mathbf{v}, t)$ tends to $\delta_{k''\bar{k}''} \delta_{k'\bar{k}'}$, yielding Eq. (3.12).

Using more accurate models for the matrix elements $V_{kk'}^a(\mathbf{R})$, in Eq. (3.8), $L_{\bar{k}'\bar{k}''}^{k'k''}(\mathbf{v}, t)$ produces another broadening component to Eq. (3.20) that seems to affect negligibly the high-energy behavior of the electron energy distributions.

-
- [1] H. D. Hagstrum, *Inelastic Ion-Surface Collisions* (Academic, New York, 1977), p. 1.
- [2] R. Monreal and S. P. Apell, Nucl. Instrum. Methods Phys. Res. B **83**, 459 (1993); R. Monreal and N. Lorente, Phys. Rev. B **52**, 4760 (1995).
- [3] B. L. Burrows, A. T. Amos, Z. L. Miskovic, and S. G. Davison, Phys. Rev. B **51**, 1409 (1995).
- [4] M. A. Vicente Alvarez, V. H. Ponce, and E. C. Goldberg, Phys. Rev. B **57**, 14919 (1998).
- [5] R. A. Baragiola and C. A. Dukes, Phys. Rev. Lett. **76**, 2547 (1996); P. Riccardi, P. Barone, A. Bonanno, A. Oliva, and R. A. Baragiola, *ibid.* **84**, 378 (2000); P. Barone, A. Sindona, R. A. Baragiola, A. Bonanno, A. Oliva, and P. Riccardi, Nucl. Instrum. Methods Phys. Res. B **209**, 68 (2003).
- [6] G. D. Mahan, Phys. Rev. **163**, 612 (1967); P. Nozieres and C. T. De Dominicis, *ibid.* **178**, 1097 (1969).
- [7] P. H. Citrin, G. K. Wertheim, and Y. Baer, Phys. Rev. Lett. **35**, 885 (1975); G. K. Wertheim, D. M. Riffe and P. H. Citrin, Phys. Rev. B **45**, 8703 (1992).
- [8] P. J. Jennings, R. O. Jones, and M. Weinert, Phys. Rev. B **37**, 6113 (1998).
- [9] A. E. S. Green, D. L. Sellin, and A. S. Zachor, Phys. Rev. **184**, 1 (1969).
- [10] P. Nordlander and J. C. Tully, Phys. Rev. B **42**, 5564 (1990);
- [11] A. Sindona and G. Falcone, Surf. Sci. **529**, 471 (2003).
- [12] P. W. Anderson, Phys. Rev. **124**, 41 (1961); D. M. News, *ibid.* **178**, 1123 (1969).
- [13] R. A. Baragiola, *Low Energy Ion-Surface Interaction* (Wiley,

- New York, 1994), p. 187.
- [14] K. Othaka and Y. Tanabe, *Rev. Mod. Phys.* **62**, 929 (1990).
- [15] R. Brako and D. M. Newns, *Rep. Prog. Phys.* **52**, 655 (1989).
- [16] L. P. Kadanov and G. Baymn, *Quantum Statistical Mechanics* (Benjamin, New York, 1962); R. Mattuck, *A Guide to Feynmann Diagrams in the Many-Body Problem*, 2nd ed. (McGraw-Hill, New York, 1976); G. D. Mahan, *Many Particle Physics* (Plenum, New York, 1981); J. W. Negele and H. Orland, *Quantum Many-Particle Systems* (Addison-Wesley, Reading, MA, 1988).